

An Automatic Optical Imaging System for Birefringent Media

Author(s): A. M. Glazer, J. G. Lewis and W. Kaminsky

Reviewed work(s):

Source: *Proceedings: Mathematical, Physical and Engineering Sciences*, Vol. 452, No. 1955 (Dec. 8, 1996), pp. 2751-2765

Published by: [The Royal Society](#)

Stable URL: <http://www.jstor.org/stable/52868>

Accessed: 09/10/2012 15:27

Your use of the JSTOR archive indicates your acceptance of the Terms & Conditions of Use, available at <http://www.jstor.org/page/info/about/policies/terms.jsp>

JSTOR is a not-for-profit service that helps scholars, researchers, and students discover, use, and build upon a wide range of content in a trusted digital archive. We use information technology and tools to increase productivity and facilitate new forms of scholarship. For more information about JSTOR, please contact support@jstor.org.



The Royal Society is collaborating with JSTOR to digitize, preserve and extend access to *Proceedings: Mathematical, Physical and Engineering Sciences*.

An automatic optical imaging system for birefringent media

BY A. M. GLAZER, J. G. LEWIS AND W. KAMINSKY

*Department of Physics, Clarendon Laboratory, University of Oxford,
Parks Road, Oxford OX1 3PU, UK*

A new optical microscope imaging system is described. The instrument is capable of producing coded colour images of an optically birefringent material, where the colour represents either $|\sin \delta|$, a function of the optical retardation; ϕ , the orientation of a section of the optical indicatrix; or I_o , the transmittance, at any place within the image. Thus the contrast normally seen in a standard crossed-polars experiment is separated out into its components. The technique is both qualitative and quantitative. Examples of the application of this system to crystals, a rock section and a biological specimen are given.

1. Introduction

Most transparent solids, including crystals, polymers, glasses and biological material, are optically anisotropic; that is the refractive index varies with the direction of vibration of light. The anisotropy arises, in the main, from the directionality of atomic or molecular arrangements or from strain. This variation of refractive index may be represented by a surface called the *indicatrix*, which has the general form of an ellipsoid. The difference between any two ellipsoid axes is the linear *birefringence* (simply called birefringence hereafter) for light directed along the third axis. For any general direction of the light, an elliptical cross-section of the indicatrix is observed, the anisotropy then being given by the difference in length of the ellipse axes. Figure 1 shows such an elliptical section, where the refractive indices are n_1 and n_2 , and the slow direction (largest refractive index) is oriented at an angle ϕ from the horizontal. The optical anisotropy of this section can then be represented by the phase shift δ of the light, given by

$$\delta = \frac{2\pi}{\lambda} \Delta n L. \quad (1.1)$$

Here, λ is the wavelength of the light, L the thickness of the specimen and $\Delta n = n_1 - n_2$. $\Delta n L$ is known as the *optical retardation*.

Probably the most well known way to observe retardation is to place the specimen between crossed linear polars in a microscope. The crossed polars ensure that light entering the microscope is not transmitted except when a birefringent specimen is inserted between the polars, whereupon striking colours are observed (see any of the textbooks on crystal optics, such as that by Hartshorne & Stuart (1970)). Furthermore, rotation of the specimen shows the well known characteristic ‘extinction’ of the transmitted light waves every 90° (in the absence of pleochroism). There

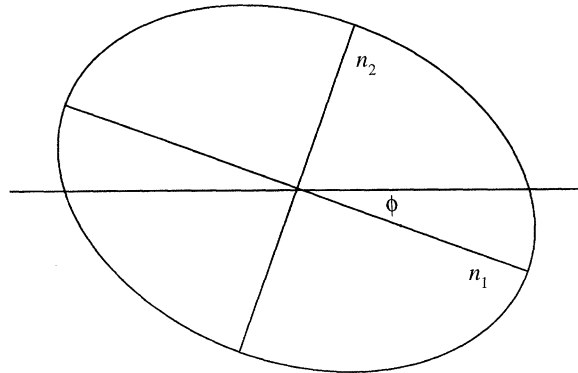


Figure 1. The optical indicatrix. ϕ is the angle between the horizontal direction and the slow (larger refractive index n_1) vibration direction of the light.

are many well established methods for measuring the retardation, such as by using compensating optical elements.

The intensity of the light through a conventional LP-S-LA (linear polarizer-specimen-linear analyser) system is given by the formula (Born & Wolf 1975)

$$I = I_0 \sin^2 2\phi \sin^2 \delta/2, \quad (1.2)$$

where I_0 is the intensity of the incident light (modified by absorption, and so can be taken to be proportional to the transmittance of the light through the specimen). Equation (1.2) then forms a useful basis for measuring the relative optical retardation of a material, say, as a function of temperature. However, it suffers from the disadvantage that the angle ϕ must first be fixed by rotating the specimen to a particular orientation with respect to the LP-S-LA arrangement: it is usual to set the orientation so that $\phi = 45^\circ$.

An alternative approach is to make use of circular polarizers instead of linear polarizers. As with two linear polarizers, two circular polarizers of opposite sense do not permit light to pass through except when a birefringent sample (which creates elliptically polarized light) is inserted between them. Such a circular polarizer-specimen-circular analyser arrangement (CP-S-CA) has the advantage that the specimen can be oriented at any angle.

Wood & Glazer (1980) described a different method of measuring the relative optical retardation by using a modulation technique. (The use of modulation techniques in polarization microscopy is well known, see for example the papers by Allen *et al.* (1963) and by Benard & Walker (1976).) In this set-up, a combination of linear polarizer and quarter-wave plate produces circularly polarized light below the specimen in a microscope. This circularly polarized wave passes through the specimen, and, if this is optically anisotropic, the light wave is converted to elliptical polarization. The light then passes through a linear analyser, which is made to rotate about the microscope axis at a frequency ω (alternatively, a suitable optical modulator crystal can achieve the same effect). The intensity through this CP-S-RLA (circular polarizer-specimen-rotating linear analyser) system is measured by a photomultiplier, and is then given by the formula

$$I = \frac{1}{2} I_0 [1 + \sin 2(\omega t - \phi) \sin \delta], \quad (1.3)$$

where t is time. Thus the result is a sinusoidal (in time) wave whose amplitude is

modulated by the term $\sin \delta$. This signal lends itself easily to electronic processing. For instance, an amplitude proportional to $\sin \delta$ can be obtained by using a phase-sensitive detector set up to extract the signal at a frequency of 2ω . The phase angle ϕ can be adjusted electronically, thus obviating the need to set the specimen in any particular orientation during the measurement. If now the sample is altered in some way, typically by heating it, the retardation changes. To see the effect of this, the term proportional to $\sin \delta$ can be plotted on a chart-recorder. Thus, for example, if one is studying a crystal that undergoes a phase transition from a birefringent (optically anisotropic) state to a non-birefringent (optically isotropic) state, an oscillating set of fringes is observed with change in temperature, which vanish at the transition temperature. Then, simply by counting the maxima and minima, one can obtain a graph of δ (and hence Δn , assuming the change in L is negligible) against temperature.

It was found (Wood & Glazer 1980) with this set-up that changes in retardation can be measured to a precision of 1 part in 10^7 , thus making the method one of the most sensitive techniques known for measuring optical changes. This rotating-analyser equipment has subsequently been used for many years to study phase transitions in a large number of compounds, both in our laboratory and elsewhere, and has provided an important contribution to the understanding of order parameters in ferroelectric and ferroelastic crystals (Wood *et al.* 1980). It has also proved to be of general importance in the study of optical properties of materials of technological interest.

Since this system senses both the *optical anisotropy*, through the quantity $\sin \delta$, and the *optical orientation* of this anisotropy, through the angle ϕ , it forms a most versatile instrument. In addition to changing the optical characteristics of the specimen by temperature, pressure, magnetic field, etc., if the specimen is translated across the field of view, with a pin-hole diaphragm inserted into the image plane of the microscope, a signal proportional to optical changes *spatially* across the specimen is obtained. This can be used to form a highly sensitive two-dimensional image of the optical anisotropy or optical orientation of the specimen (Wadhawan *et al.* 1992). However, such a method is extremely time-consuming.

In this paper, we show how this modulation technique can be used to make a novel microscope imaging system (UK patent application number BG9604785.7) in which the contrast (expressed in coded colours) seen in the image is a measure of optical anisotropy ($|\sin \delta|$), optical orientation (ϕ) or transmittance (I_o). Thus this instrument is capable of automatically separating the three terms that normally contribute to the usual crossed-polars image given by equation (1.2). A similar system for separating optical anisotropy and orientation has recently been published by Oldenbourg & Mei (1995), who used a CP-S-CA arrangement, in which the circular polarization of one of the components is altered to form different images. These images are then processed to separate out the two effects on the assumption that the retardation is small. This system is very sensitive to small retardations, but is inaccurate for retardations greater than 1/25th of a wavelength, whereas our system, in which no such assumption is made, is quantitative over all ranges of retardation.

2. Description of imaging technique

The experimental arrangement for the new imaging system is shown schematically in figure 2. The set-up is similar to the earlier rotating-analyser system, except that

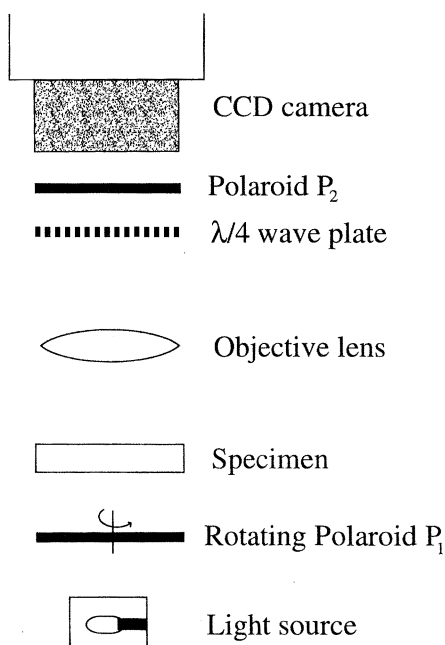


Figure 2. A schematic diagram of the imaging microscope.

we have changed the order of the optical components to place a rotating polarizer, consisting of a conventional Polaroid (P_1), below the microscope sub-stage and a circular analyser, consisting of a quarter-wave plate and a Polaroid (P_2) at the 45° position, above. This ensures that P_1 lies far from the image plane of the microscope so that any defects in the Polaroid are not imaged. A video CCD camera (IK-M48PK Toshiba, single-chip colour camera) is attached to the camera port of the microscope (Reichert Zetopan), with the chip at the primary image plane of the objective. It is best in this application, especially if quantitative measurements are to be obtained, that monochromatic light (such as from a sodium emission lamp, or white light with a suitable filter) is used with a quarter-wave plate specifically made for that particular wavelength. In practice, the high sensitivity of this apparatus is such that it is necessary to make fine adjustments to obtain the exact 45° angle for the circular analyser. To do this we monitor the intensity through the system without a specimen in place while P_1 is rotated. The angle between the quarter-wave plate and P_2 is then adjusted carefully until the signal remains constant to within an acceptable level, corresponding to a value of $|\sin \delta| < 0.01$.

Note that the camera need not be a colour camera for this application, but that for best results it should be capable of having an intensity gamma correction factor set to 1. Our camera produces an output in analogue PAL format. The signal is fed to a Video Frame Grabber (Vision Dynamics Elvis II in 4:2:2 format) which digitizes the intensity into 8 bits in each of 1024×512 pixels for presentation on a computer monitor (in practice we use 640×480 pixels on the screen).

In order to obtain a linearized signal for computer processing, the gamma correction factor is set to 1, thus providing a linear intensity signal to the frame-grabber. However, the latter causes its own small nonlinearity and this must be corrected before further processing. To do this we apply a correction curve previously established

by varying light levels in controlled amounts through a linear polarizer with a linear analyser set to several different angles.

P_1 is rotated by a computer-controlled stepper motor; however, instead of rotating it continuously as in the earlier paper of Wood & Glazer, it is stepped to fixed angles and complete images are captured at each step via the frame grabber. (Note that instead of physically rotating a Polaroid, the same effect can also be achieved with modulating crystals).

The digital output from the frame-grabber is accessed by a PC and is processed before displaying on the screen. A live image of the specimen can be observed on the computer screen, thus making it easy to set the specimen into a particular position before carrying out the rotating polarizer measurements.

In order to form the three images (anisotropy, orientation, transmittance), the processing procedure separates out the three components from equation (1.3). To do this we measure the intensity at each pixel position for several equal polarizer P_1 angles, typically six angles of 30° each. Equation (1.3) can be recast in the form:

$$I = \frac{1}{2}I_o + \frac{1}{2}I_o \sin \delta \cos 2\phi \sin 2\omega t - \frac{1}{2}I_o \sin \delta \sin 2\phi \cos 2\omega t. \quad (2.1)$$

The derivation of the quantities of interest is achieved by a least-squares fitting procedure to the equation:

$$y(x) = a_0 + a_1 \sin x + a_2 \cos x, \quad (2.2)$$

where, by comparison with equation (2.1),

$$a_0 = \frac{1}{2}I_o, \quad a_1 = \frac{1}{2}I_o \sin \delta \cos 2\phi, \quad a_2 = -\frac{1}{2}I_o \sin \delta \sin 2\phi. \quad (2.3)$$

If data for P_1 stepped through a total of 180° are accumulated, the parameters a_i can be described simply by

$$a_0 = \sum_{i=1}^N \frac{1}{N} y_i, \quad a_1 = \sum_{i=1}^N \frac{2}{N} y_i \sin x_i, \quad a_2 = \sum_{i=1}^N \frac{2}{N} y_i \cos x_i, \quad (2.4)$$

where N is the number of angles stepped through.

From equations (2.3), the amplitude, corresponding to the optical anisotropy is then given by

$$|\sin \delta| = \frac{(a_1^2 + a_2^2)^{1/2}}{a_0} \quad (2.5)$$

and the orientation angle between 0 and 180° by

$$\phi = \frac{1}{2} \arcsin \left(-\frac{a_2}{(a_1^2 + a_2^2)^{1/2}} \right), \quad (2.6 a)$$

or

$$\phi = \frac{1}{2} \arccos \left(+\frac{a_1}{(a_1^2 + a_2^2)^{1/2}} \right). \quad (2.6 b)$$

In practice, we use either equation (2.6 a) or (2.6 b) to obtain ϕ , depending on whether a_1 is larger or smaller than a_2 (this procedure minimizes the error in determining ϕ). In addition, the quantity a_0 , which is a measure of the DC offset of the oscillating signal, is also obtained and gives the transmittance I_o of the light. Note that because this is separated out automatically in the refinement process, variations in lamp intensity across the field of view are eliminated entirely from the calculations

of $|\sin \delta|$ and ϕ . The plot of I_o , on the other hand, may include such variations, but these can be eliminated, if required, by carrying out a background run without a sample in place. In practice, however, we have found this to be unnecessary in our system.

The present measurement technique enables the images (640×480 pixels) to be formed with the minimum of background noise. Using a 100 MHz Pentium PC with six angular steps of the polarizer, we find with our present software that the time required to collect the data and process them to obtain the three images representing anisotropy ($|\sin \delta|$), orientation (ϕ) and transmittance (I_o), is approximately 40 s. The resulting coded colour images are stored as PCX files.

To display the images, in the present system we use 100 colours for the $|\sin \delta|$ terms, thus giving a resolution of 0.01 \dagger (for Na light this corresponds to a resolution in retardation of approximately 1 nm). For the ϕ orientation images 180 colours are used, giving a resolution of 1°. These resolutions are principally determined by the fact that the frame grabber only produces an 8-bit output, which nevertheless gives a gain in precision over conventional compensator measurements of about an order of magnitude (a 16-bit frame grabber with a CCD camera of very high signal-to-noise ratio, would result in a gain in resolution by another factor of 256: in such a case in order to take advantage of this, it would be necessary to use better polarizing elements than Polaroid). We find that the use of colour has significant advantages over a grey scale, where the slow change of intensity makes it difficult to see small changes from pixel to pixel. The colour palette adopted in the present work will be shown below next to each image. In this palette, there is no black and white, these being reserved for certain special cases:

1. If the light intensity becomes too low, typically when the region being examined is strongly absorbing, equation (1.3) cannot be solved. Pixels in such a region are then automatically set to black.

2. Whenever $|\sin \delta|$ becomes close to zero the angle ϕ becomes indeterminate. This happens whenever a region is isotropic (the section of the optical indicatrix being viewed is a circle), or when the retardation is a multiple of $\lambda/2$. Pixels where this occurs ($|\sin \delta| < 0.01$ in our case) are automatically coloured white in the orientation image.

In order to be able to interpret the coded-colour images, it is necessary to know what the value is of each coloured pixel. A convenient way to do this is to scan manually through the colour palette at the same time illuminating only those pixels with the selected colour (and hence value of $|\sin \delta|$ or ϕ). Another useful facility is the ability to present a histogram of numbers of pixels against colour value.

Finally, it should be realized that, because it is $|\sin \delta|$ that is obtained at any point in the image, it is not possible to know how many periods (known as the *order*) of the sine function have been passed through, unless other information is supplied. The easiest way to solve this is to use a standard compensating plate with white light. A quick observation of this type will then suffice to determine the order within which the retardation value lies. Carrying out the measurements at two or more wavelengths can also be used to help in determining the order.

In addition, equation (1.3) ignores the presence of optical effects such as linear and circular dichroism and optical gyration. Of these, optical gyration and circular

\dagger We have recently extended the palette to 200 colours thus changing the $|\sin \delta|$ resolution to 0.005.

dichroism need not be considered, since they are normally[‡] only seen directly in isotropic sections where $|\sin \delta| = 0$ and ϕ is indeterminate. The presence of linear dichroism is of more concern, although for most materials it can be considered to be a small effect. We have recently derived a modified version of equation (1.3) by including this effect, and it is hoped at a later date to use this to enable linear dichroism to be separated out and a corresponding image to be created. Details will be published in due course.

3. Examples of images

To illustrate the versatility and use of this new imaging technique, we show five typical examples, two in the field of crystallography, one in earth sciences and one in biology. All the images shown are made at the same magnification, with the vertical dimension equivalent to a distance of 1.2 mm in the specimen. Each image was made with a X5.5, NA = 0.15 microscope objective. In each case, Na light from an emission tube was used. The apparatus was set up so that the orientation $\phi = 0^\circ$ (the direction of the slow axis) is horizontal in the orientation images, with angles increasing clockwise from this position. The background retardation in all cases was $|\sin \delta| < 0.01$.

(a) *Twinning in barium titanate*

The perovskite crystal BaTiO₃ is a well known ferroelectric material which has many interesting physical properties that make it useful for dielectric, optical, pyroelectric and piezoelectric applications. On cooling from its cubic high-temperature phase it undergoes a phase transition to the room-temperature tetragonal phase. This results in three tetragonal twin domains (*c*-axes along each of the pseudocubic axes).

Figure 3*a* shows the $|\sin \delta|$ image of part of a flux-grown crystal of BaTiO₃. It is important to note that this was a crystal selected at random, no special care being taken to polish the surfaces or prepare the specimen in any way. This image clearly shows two regions, one mainly coloured blue and the other with coloured contours. Since this image emphasises the effect of strain within the crystal, it is clear that the second type of domain shows more strain variation than the first. Note, also that the strain appears to show some periodicity along the domains.

The irregularity of the walls in these domains deserves mention. Such peculiar patterns were first observed by Forsbergh (1949), who found several remarkable and complex domain contrast effects in optical images of BaTiO₃. These were interpreted in terms of the intersections of groups of twin lamellae to form truncated laminated pyramids (figure 18 in Forsbergh's paper shows a domain pattern very similar to that seen in our sample).

Figure 3*b* shows the corresponding orientation image. The two types of domain are now coloured grey and maroon, respectively. By scanning through the colour range, we find that the maroon regions have $\phi = 0^\circ$ (slow direction pointing east–west), and that the grey regions have $\phi = 90^\circ$ (slow direction pointing north–south), thus immediately showing that the two types of domain are at right angles to each other.

[‡] The observation of gyration and circular dichroism in birefringent sections requires specialized instruments (see, for example, Moxon & Renshaw 1990) because the effect of optical retardation is normally many orders of magnitude greater than the effect of gyration.

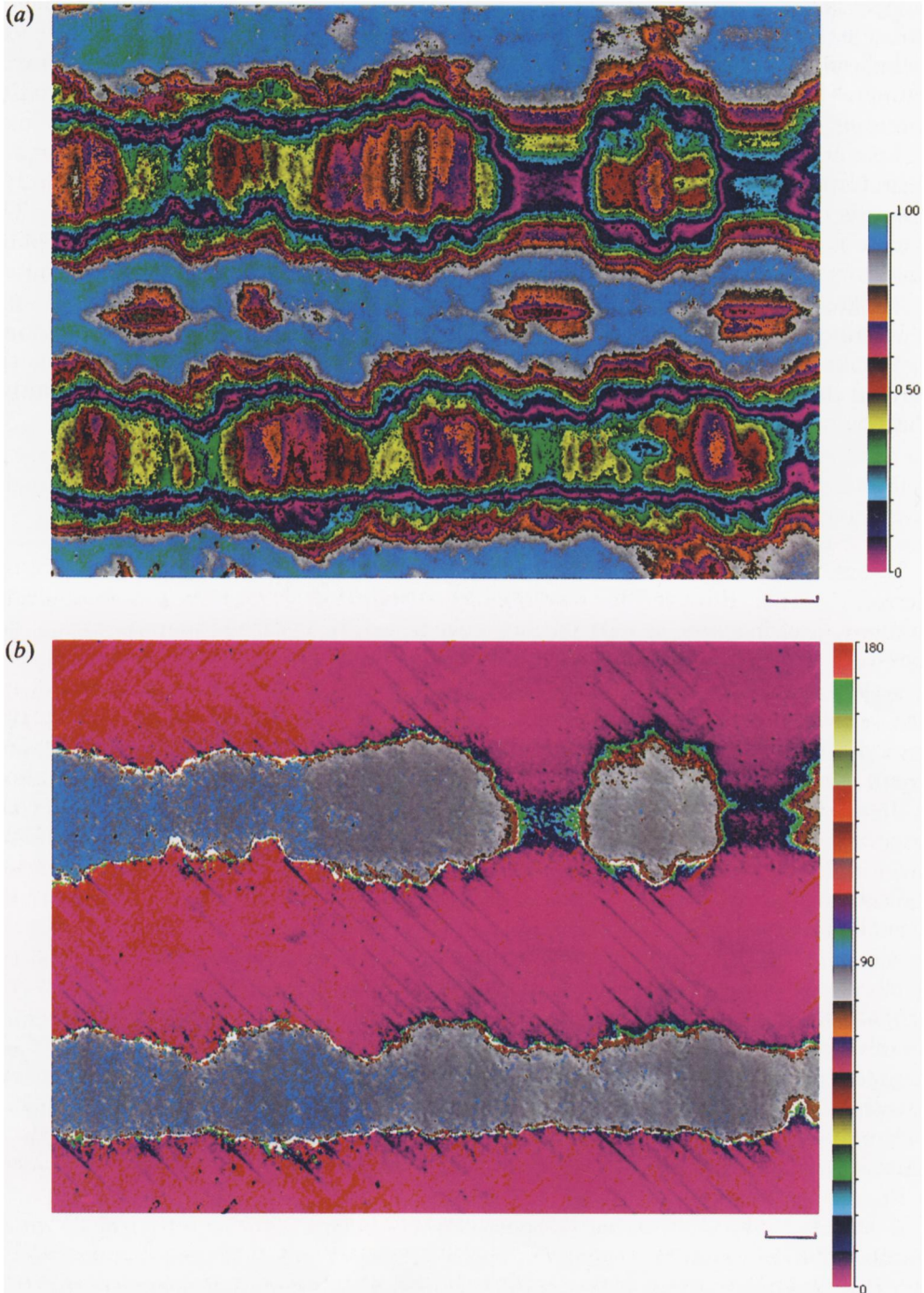


Figure 3. (a) $|\sin \delta|$, retardation image of a crystal of flux-grown BaTiO₃ (thickness 0.3 mm). The colour scale for $|\sin \delta|$ is shown on the right-hand side. The horizontal scale bar (bottom right) is 0.1 mm. (b) Orientation image of BaTiO₃ crystal. The colour scale for orientation is shown on the right-hand side.

Since it is known that in BaTiO_3 the indicatrix is optically negative the tetragonal c -axis must lie perpendicular to the slow direction and so we determine that the c -axis lies parallel to the domain walls in the grey regions. The clear differences between figures 3a and 3b show how well the imaging technique has separated the orientation contrast from that due to retardation.

Note too that the change of orientation enables us to identify a sign change in $\sin \delta$. Consider the variation in $|\sin \delta|$ along a trajectory from the centre of figure 3a upwards to the grey-white bars in the middle of the domain that has $\phi = 90^\circ$. The change in orientation means that if we take $\sin \delta \approx +0.9$ (light blue) in the middle, $\sin \delta$ drops to zero (purple) and then changes sign eventually becoming approximately -0.8 (grey bars); i.e. the change is continuous.

Finally, in figure 3b (but not in figure 3a), fine cross-hatch lines can be discerned in the maroon regions. These too can be observed in Forsbergh's (1949) paper: the present results show that these particular features are orientational in origin rather than being due to retardation differences.

(b) Synthetic diamond

Diamond belongs to the cubic crystal system, and as such is expected to be optically isotropic. However, it is well known that it does in fact show a weak strain-induced birefringence, associated particularly with growth sector boundaries, dislocations and defects. Figures 4a and b show the $|\sin \delta|$ and orientation images of a synthetic diamond (this sample, labelled HS, was also the subject of an X-ray topography study by Kowalski *et al.* (1996)) looking down the $[111]$ direction. It is immediately apparent that there is an approximate three-fold symmetry in the $|\sin \delta|$ image, consistent with the symmetry of this direction in the crystal. The sharp lines in the form of a 'Y' bisecting the three 'heart-shaped' regions are very thin 110 growth sectors between slices through (100), (010) and (001) faces (see Lang (1994) for a full description of these types of growth sectors). At the same time, the retardation can be seen to drop to zero (purple colour) in the three regions between the growth sector boundaries.

The progression of colours in the orientation image is such that the slow axis is 0° on the left side and then rotates clockwise about the intersection point of the growth sector boundaries, becoming $180 = 0^\circ$ again on the right side. This gives an effective two-fold symmetry, which has nothing to do with the symmetry of the crystal. Near the centre of the figure, sharp changes in orientation are observed half way between the growth sector lines of figure 4a (where $|\sin \delta|$ drops towards zero) i.e. 60° round from the growth sectors. The white colours in these regions indicate that the indicatrix section in these regions is circular and hence ϕ becomes indeterminate here.

Figure 4c shows the computed transmission image (I_o). This too shows an approximate three-fold symmetry around the junction of the growth sector boundaries. The colour scale in this case is purely arbitrary. Despite this obviously non-uniform background variation, the $|\sin \delta|$ and orientation images are not affected. This variation in light transmission is known to be due to two factors, a zonal variation in population density of small non-diamond bodies in the crystal, and also a zonal variation and growth-sectorial dependence of the optical absorption produced by nitrogen impurity (Lang *et al.* 1995).

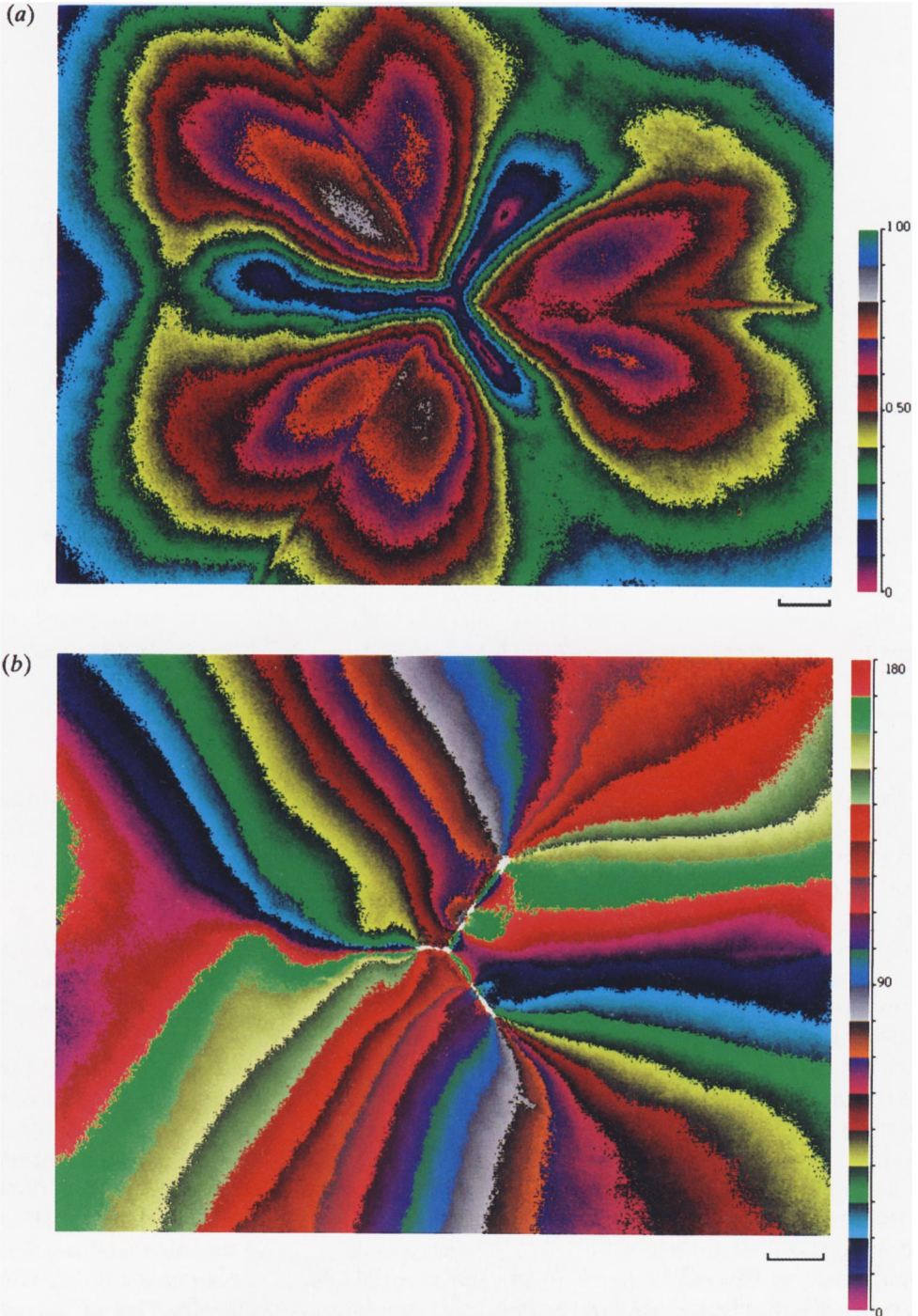


Figure 4. (a) $|\sin \delta|$, retardation image of a synthetic diamond crystal (specimen HS, thickness 0.4 mm) viewed along $[111]$. The horizontal scale bar (bottom right) is 0.1 mm. (b) Orientation image of synthetic diamond crystal.



Figure 4. (c) Transmission image of synthetic diamond crystal. (Colour scale corresponds to increasing transmission vertically upwards.)

(c) *Twinning in anorthosite*

Figure 5a shows a $|\sin \delta|$ image of part of a rock section of Ameralik anorthosite. The largest region is of particular interest, since it shows one of the typical twinning forms found in plagioclases (horizontal domains in the figure). A survey of all the crystal grains in the section with conventional cross-polar techniques showed that the domains in almost all the crystal grains become equally illuminated at 45° to the polars, indicating that they are albite twins with the sections of the samples cut approximately normal to $\{010\}$ (Cox *et al.* 1967; Deer *et al.* 1995). In figure 5a, these domains are coloured yellow/red/purple, corresponding to $|\sin \delta|$ between 0.4 and 0.6 approximately.

Of particular interest is the fact that the domain walls are clearly of a different colour, showing that they have a well-defined $|\sin \delta|$ of their own equal to about 0.3. This may indicate the occurrence of strain at the domain wall boundaries, which will tend to alter the retardation rather than the orientation. Alternatively, it may be due to the domain walls not being vertical, with light traversing the two twin structures in succession (with high magnification under crossed polars, the walls, however, do not appear to move with changing focus, suggesting that the amount of tilting is too small to cause this effect; in addition, almost all the other grains in the rock section show identical effects). As far as we know, this has not been observed before, and other experiments, involving tilting of the specimen, will be necessary to investigate the cause of the effect.

Figure 5b shows the orientation image. The different mineral grains are clear, the strong colour changes indicating grains in very different orientations. The albite

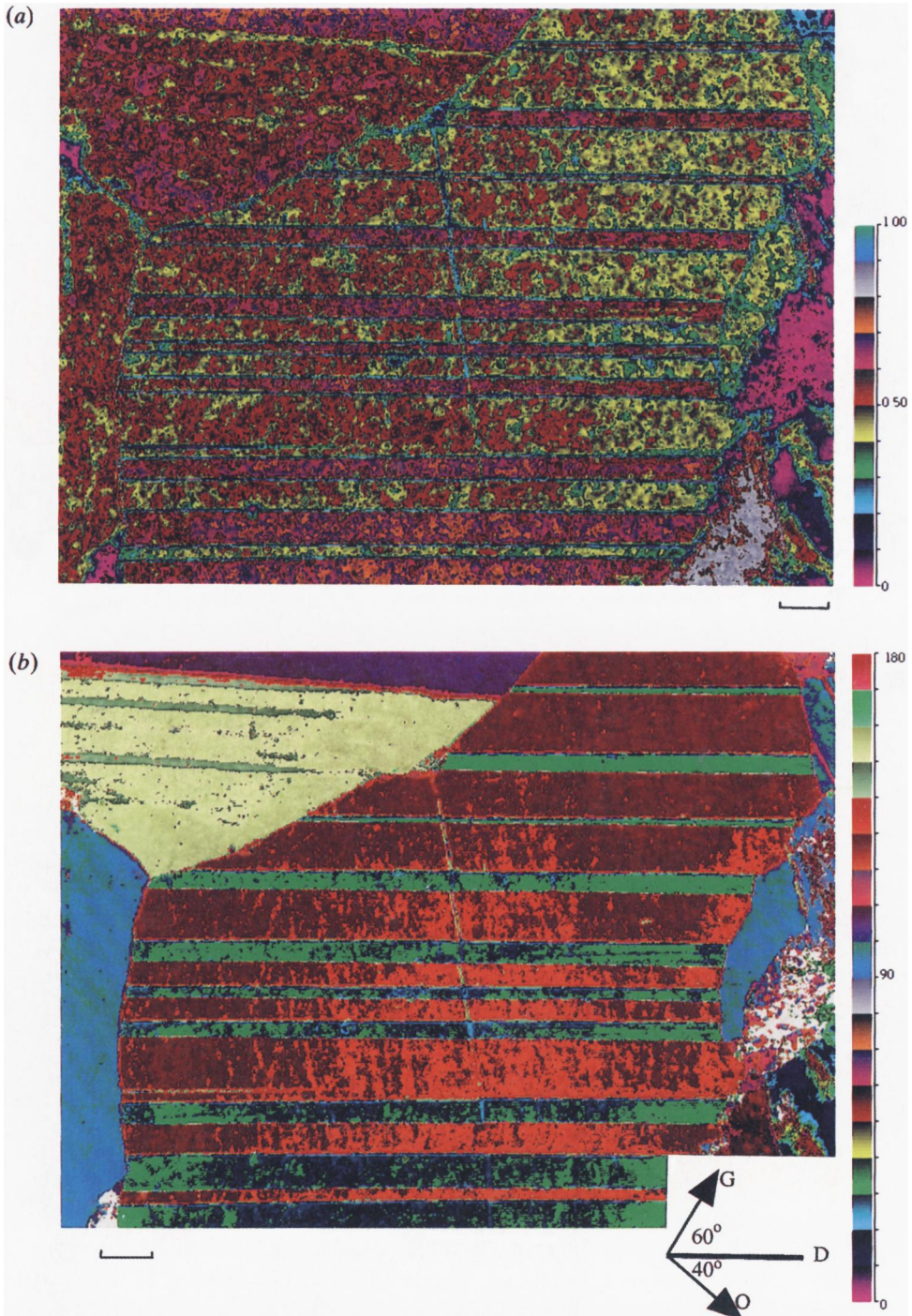


Figure 5. (a) $|\sin \delta|$, retardation image of a section of Ameralik anorthosite (thickness 0.03 mm). The horizontal scale bar (bottom right) is 0.1 mm. (b) Orientation image of section of Ameralik anorthosite. The inset diagram indicates the directions of the domain walls (D), and the fast axes (G, green; O, orange) of the albite twin domains. The other major grains are at the following angles with respect to $\phi = 0^\circ$: purple grain at top left, 105° ; light yellow grain, 152° ; blue grain at left, 95° .

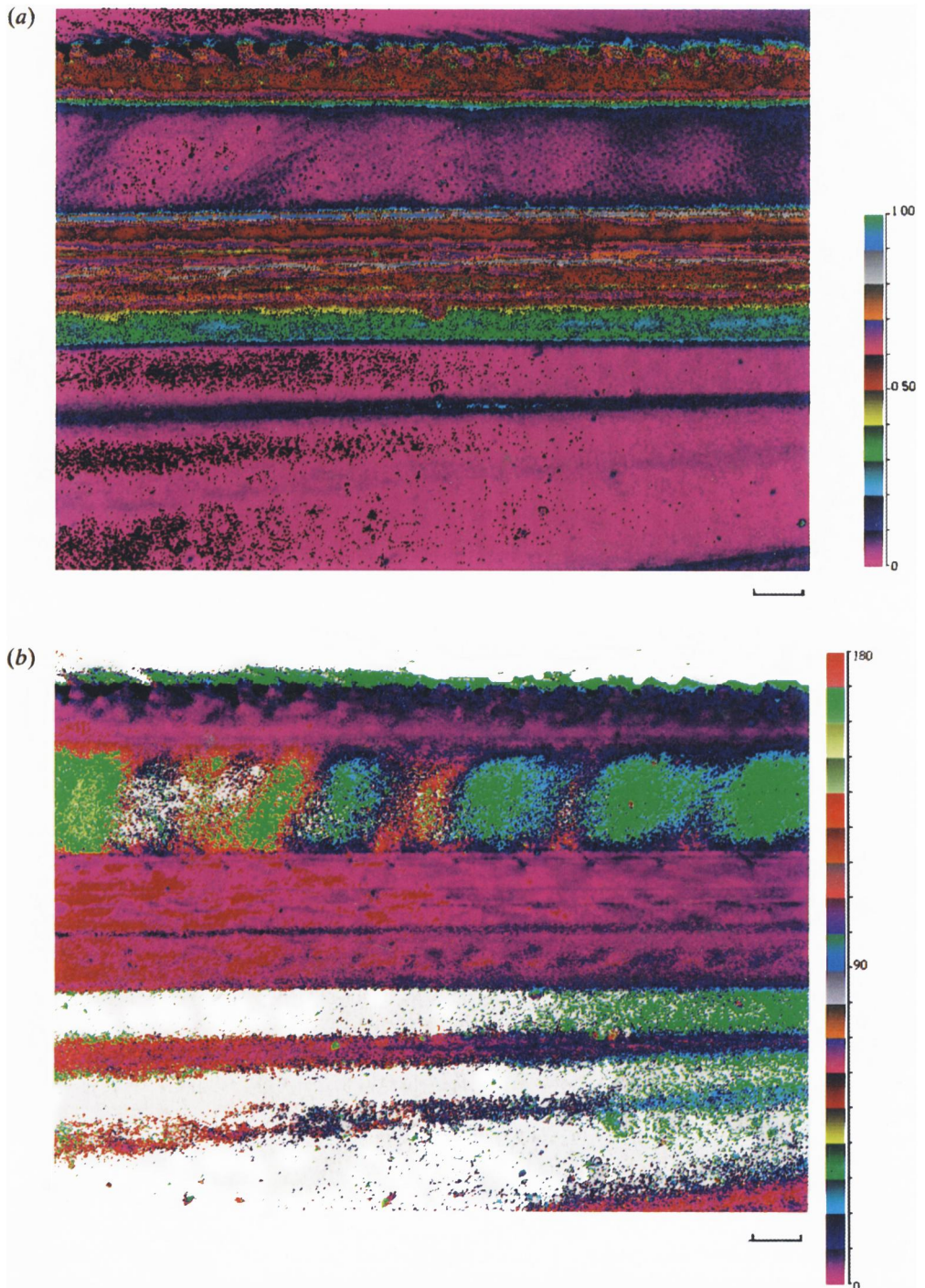


Figure 6. (a) $|\sin \delta|$, retardation image of crane-fly wing. The leading edge is horizontally along the top of the diagram. The horizontal scale bar (bottom right) is 0.1 mm. (b) Orientation image of crane-fly wing. The white regions are those for which $|\sin \delta|$ is less than 0.01 and thus make the determination of ϕ inaccurate.

twins are coloured green and orange, corresponding to ϕ of 30° and 130° , respectively. The inset diagram shows these directions with respect to the domain walls (the fast axes are 60° and 40° , respectively). The slow directions are not quite symmetrically disposed with regard to the domain walls, showing that the domain walls in this particular grain are not absolutely vertical out of the plane of the crystal. Nevertheless, they are sufficiently close to the vertical to enable one to estimate the composition of the crystal. From the above, the average extinction angle for the fast axes is $(60 + 40)/2 = 50^\circ$. We found that this extinction angle was the largest among all the grains examined, and this makes it diagnostic of the actual composition of the plagioclase. According to the standard graphs (see, for example, Deer *et al.* 1995, p. 447) the measurement suggests that the sample is close to 80–90% anorthite. The imaging system therefore makes routine analysis of many grains in this way relatively quick and simple.

(d) Crane-fly wing

Figure 6 shows an image of a small portion of the leading edge (across the top of the figure) of a crane-fly wing. In the $|\sin \delta|$ image, the maroon colour over most of the image corresponds to a low value of $|\sin \delta|$ of about 0.00–0.02. The other colours are of higher $|\sin \delta|$, e.g. the blue-green band corresponding to one of the veins is approximately 0.35 and the yellow band approximately 0.45. However, since the birefringence of a sample like this is very small, all the values of $|\sin \delta|$ are of first order and it is therefore a simple matter to calculate the absolute values of δ . Hence, knowing the thickness of the wing, the refractive index difference Δn could be computed.

The corresponding orientation image (figure 6*b*) is particularly interesting in the observation of a series of approximately equally spaced patches, coloured green, along the band close to the leading edge of the wing. This band, as seen in figure 6*a*, is of *constant* low retardation. The green patches have their slow axes pointing approximately at 35° clockwise from the horizontal. The origin of this curious clockwise twisting is unknown and deserves further study.

4. Conclusions

We have demonstrated that by combining a rotating plane of polarization with a circular analyser, it is possible to separate successfully the terms $|\sin \delta|$ (a measure of optical anisotropy), ϕ (optical orientation) and I_o (transmittance). By using a CCD camera system we have been able to obtain high-resolution images in which these quantities provide the contrast represented by coded colours. In addition, it has been possible to obtain numerical results from the images, thus making the technique both qualitative and quantitative at the same time. The large variety of materials that can be processed in this way, as provided by the above examples, shows that this new imaging system is a potentially important research tool for the study of optical anisotropy in many disciplines. Finally, we should point out that this technique is not confined to microscopy, but could be applied equally to any situation where birefringence is of interest, such as in engineering applications where plastic model constructional elements observed between crossed polars are submitted to load forces in order to determine regions of strain.

We thank Oxford Cryosystems for support. J.G.L. is grateful also to the Engineering and Phys-

ical Sciences Research Council for a CASE studentship. We thank Dr P. A. Thomas (Warwick University) for helpful advice. We thank Dr K. G. Cox (Earth Science, Oxford) for the anorthosite specimen and advice on albite twinning, Dr S. Simpson (Zoology, Oxford) for the crane-fly specimen and Dr M. Moore (Physics, Royal Holloway College, London) for the diamond.

References

- Allen, R. D., Brault, J. & Moore, R. 1963 *J. Cell. Biology* **18**, 223–235.
- Benard, D. J. & Walker, W. C. 1976 *Rev. Sci. Instrum.* **47**, 122–127.
- Born, M. & Wolf, E. 1975 *Principles of optics*. New York: Pergamon.
- Cox, K. G., Price, N. B. & Harte, B. 1967 *An introduction to the practical study of crystals, minerals and rocks*. London: McGraw-Hill.
- Deer, W. A., Howie, R. A. & Zussman, J. 1995 *An introduction to the rock-forming minerals*. London: Longman.
- Forsbergh, P. W. 1949 *Phys. Rev.* **76**, 1187–1201.
- Hartshorne, N. H. & Stuart, A. 1970 *Crystals and the polarizing microscope*. London: Arnold.
- Kowalski, G., Moore, M., Gledhill, G. & Maričić, Z. 1996 *J. Phys. D* **29**, 793–800.
- Lang, A. R. 1994 *J. Appl. Cryst.* **27**, 988–1001.
- Lang, A. R., Vincent, R., Burton, N. C. & Makepeace, A. P. W. 1995 *J. Appl. Cryst.* **28**, 690–699.
- Moxon, J. R. L. & Renshaw, A. R. 1990 *J. Phys.: Condens. Matter* **2**, 6807–6836.
- Oldenbourg, R. & Mei, G. 1995 *J. Microscopy* **180**, 140–147.
- Wadhawan, V. K., Somayazulu, M. S. & Sastry, P. U. M. 1992 *Indian J Pure Appl. Phys.* **30**, 729–732.
- Wood, I. G. & Glazer, A. M. 1980 *J. Appl. Cryst.* **13**, 217–233.
- Wood, I. G., Welber, B., David, W. I. F. & Glazer, A. M. 1980 *J. Appl. Cryst.* **13**, 224–229.

Received 26 July 1996; revised 11 September 1996; accepted 9 October 1996